A DNS STUDY OF REYNOLDS-NUMBER DEPENDENCE ON PRESSURE FLUCTUATIONS IN A TURBULENT CHANNEL FLOW

Hiroyuki Abe
Information Technology Center,
Japan Aerospace Exploration Agency
Jindaiji-higashi, Chofu, Tokyo 182-8522, Japan
habe@chofu.jaxa.jp

Yuichi Matsuo
Information Technology Center,
Japan Aerospace Exploration Agency
Jindaiji-higashi, Chofu, Tokyo 182-8522, Japan
matsuo@chofu.jaxa.jp

Hiroshi Kawamura
Department of Mechanical Engineering,
Tokyo University of Science
Yamazaki, Noda-shi, Chiba 278-8510, Japan
kawa@rs.noda.tus.ac.jp

ABSTRACT

DNS of a turbulent channel flow has been carried out at four Reynolds numbers, 180, 395, 640 and 1020, based on the friction velocity and the channel half width in order to investigate the Reynolds-number dependence on the pressure fluctuations. It is shown that large peaks appear in the streamwise spectra of the wall pressure fluctuations at low wavenumbers for the Reynolds numbers investigated. The origin of the peaks is examined using the pressure splitting method such as the rapid and slow parts. At higher Reynolds number, a closer examination reveals that large-scale patterns of the instantaneous wall pressure fluctuations are essentially associated with large-scale structures of the instantaneous rapid pressure in the outer layer, which causes the noticeable peaks in the wall pressure spectra at low wavenumbers.

INTRODUCTION

The behavior of pressure fluctuations in wall-bounded flows is of great importance in the prediction of sound and noise, and also in the construction of more reliable turbulence modeling. Over the past several decades, a large amount of experimental and theoretical works have been conducted, where its global characteristics have been fairly well examined (see, for example, Willmarth, 1975; Eckelmann, 1989).

On the other hand, owing to an evolution of numerical simulation technique, direct numerical simulation (DNS) enables us to investigate three-dimensional behavior of pressure at moderate Reynolds numbers. For example, Kim (1989) investigated the characteristics of pressure fluctuations in a turbulent channel flow by performing DNS at $Re_\tau = u_\tau \delta/\nu = 180$, where u_τ is the friction velocity, δ the channel half width and ν the kinematic viscosity. He examined the behavior of the linear and nonlinear terms in the Poisson equation, and showed that the contribution of the slow part is substantially larger than that of the rapid part except near the wall where the two parts are almost the same magnitude. Also, he indicated that there appears a peak in the streamwise power spectrum of the rapid pressure, which persists throughout the channel. Choi and Moin (1990) carried out DNS in a turbulent channel flow at $Re_\tau = 180$, and examined the behavior of the wall pressure fluctuations where the scaling issue was intensively discussed as compared with the existing experimental results. They showed in the frequency power spectrum that the inner scaling is appropriate for high frequencies, whereas the outer scaling is suitable for low frequencies. Johansson et al. (1991) used DNS database in a turbulent channel flow at $Re_\tau = 180$, and examined the near-wall turbulence structures with conditional sampling techniques. They showed that an intense localized high-pressure pattern is associated with the shear-layer structure. Hu et al. (1999) investigated source of sound radiation by performing DNS of turbulent Poiseuille and Couette flows with relatively large computational domains. They showed the wavenumber-frequency spectra of all the sound sources, and examined the contributions to the radiated sound intensity. However, unlike the velocity and vorticity fluctuations (Moser et al, 1999; del Álamo et al., 2004), DNS studies of the pressure fluctuations have been limited at $Re_\tau < 400$ where the Reynolds-number effects may hardly be discussed because of the low Reynolds-number effects (Antonia and Kim, 1994).

In the present study, we use our DNS database of turbulent channel flow at four Reynolds numbers, $Re_\tau = 180$, 395, 640 and 1020 (Abe et al., 2004a). The wide range of the Reynolds number enables us to evaluate the Reynolds-number dependence on the pressure fluctuations. The purpose of the

Table 1: Domain size, grid points, spatial resolution and sampling time period.

Re_τ	180	395	640	1020
$L_x \times L_y \times L_z$	$12.8\delta \times 2\delta \times 6.4\delta$	$12.8\delta \times 2\delta \times 6.4\delta$	$12.8\delta \times 2\delta \times 6.4\delta$	$12.8\delta \times 2\delta \times 6.4\delta$
$L_x^+ \times L_y^+ \times L_z^+$	$2304 \times 360 \times 1152$	$5056 \times 790 \times 2528$	$8192 \times 1280 \times 4096$	$13056 \times 2040 \times 6528$
$N_x \times N_y \times N_z$	$256 \times 128 \times 256$	$512 \times 192 \times 512$	$1024 \times 256 \times 1024$	$2048 \times 448 \times 1536$
$\Delta x^+, \Delta y^+, \Delta z^+$	$9.00, 0.20 \sim 5.90, 4.50$	$9.88, 0.15 \sim 6.52, 4.94$	$8.00, 0.15 \sim 8.02, 4.00$	$6.38, 0.15 \sim 7.32, 4.25$
Tu_m/L_x	49	50	14	20

present study is to report the Reynolds-number dependence on the pressure fluctuations as described by root-mean-square (rms) values, power spectra and instantaneous fields up to $Re_\tau = 1020$. Furthermore, the pressure splitting method such as the rapid and slow parts is adopted at $Re_\tau = 1020$ in order to examine the global phenomena of the pressure at higher Reynolds number.

NUMERICAL METHODOLOGY

The flow is assumed to be a fully developed turbulent channel flow. It is driven by the streamwise mean pressure gradient. For the time integration, a fractional step method is adopted, and a semi-implicit time advancement is used. For the viscous terms with wall-normal derivatives, the Crank-Nicolson method is used. For the other terms, the second-order Adams-Bashforth method is applied for $Re_\tau = 180$, 395 and 640, and the low storage third-order Runge-Kutta method is for $Re_\tau = 1020$. For the spatial discretization, the finite difference method is adopted. The numerical scheme with the fourth-order accuracy is applied in the streamwise and spanwise directions, while the one with the second-order is adopted in the wall-normal direction. Further detailed numerical methodology and the validation of results can be found in Kawamura et al. (1999) and Abe et al. (2001, 2004a).

The computational domain size ($L_x \times L_y \times L_z$), number of grid points ($N_x \times N_y \times N_z$), spatial resolution ($\Delta x^+, \Delta y^+, \Delta z^+$) and sampling time period (Tu_m/L_x) are given in Table 1, where T and u_m denote the sampling time and the bulk mean velocity, respectively. A relatively large domain size is employed in order to contain a few numbers of large-scale structures. Also, statistical data have been integrated in time as long as possible to discuss the low-wavenumber behavior. Note that throughout the paper, the variables u_i, p and x_i are the velocity, pressure and location, respectively, where the subscript $i = 1$, 2 and 3 indicates the streamwise, wall-normal and spanwise directions. The superscripts $+$ and $*$ represent the normalization of wall units and δ, respectively, and a prime denotes the fluctuation to the average value. The streamwise, wall-normal and spanwise velocities, u, v, and w, and the corresponding locations, x, y, and z, are also used interchangeably.

RESULTS AND DISCUSSION

The rms values of the pressure fluctuations, p'_{rms}, for $Re_\tau = 180$, 395, 640 and 1020 are normalized by the wall-shear stress τ_w, and are shown in Fig. 1. The DNS result of Moser et al. (1999) at $Re_\tau = 590$ is also included for comparison. In Fig. 1(a), the rms value increases significantly with increasing Reynolds number in terms of y^+ throughout the channel, where the peak position is located at $y^+ \approx 30$

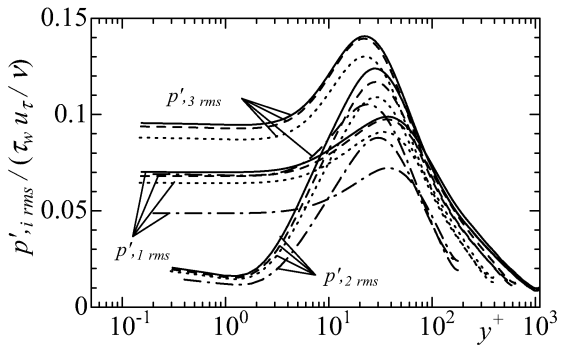

Figure 2: Root-mean-square value of the pressure derivatives normalized by $\tau_w u_\tau/\nu$ for $Re_\tau = 180$, 395, 640 and 1020. — —, $Re_\tau = 1020$; - - - - -, $Re_\tau = 640$; · · · · ·, $Re_\tau = 395$; — · —, $Re_\tau = 180$.

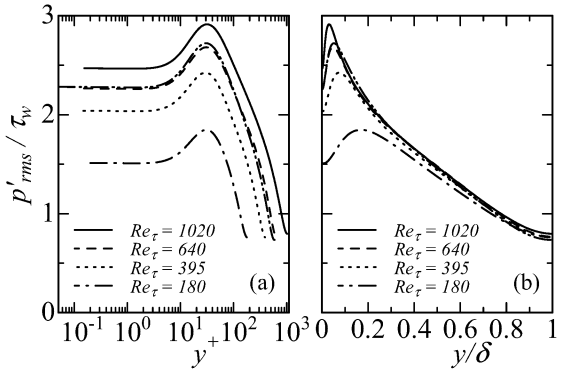

Figure 1: Root-mean-square value of the pressure fluctuations for $Re_\tau = 180$, 395, 640 and 1020: (a) inner scaling; (b) outer scaling. —··— , Moser et al. (1999) at $Re_\tau = 590$.

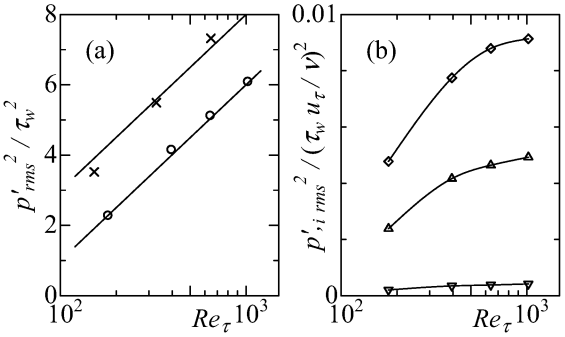

Figure 3: Near-wall limiting values of p'^2_{rms} and $p'^2_{,i\,rms}$ normalized by τ_w^2 and $(\tau_w u_\tau/\nu)^2$, respectively, as a function of the Reynolds number: (a) p'^2_{rms}; (b) $p'^2_{,i\,rms}$. ○, p'^2_{rms}; △, $p'^2_{,1\,rms}$; ▽, $p'^2_{,2\,rms}$; ◇, $p'^2_{,3\,rms}$; ×, p'^2_{rms} of Spalart (1988).

independently of Re_τ. The peak position corresponds to the location where the source terms in the Poisson equation show the largest value (Kim, 1989). In Fig. 1(b), on the other hand, the rms value is almost collapsed at $y/\delta > 0.2$ in terms of y/δ, suggesting the suitability of the outer scaling in the outer layer.

Figure 2 shows three components of the rms pressure derivatives, $p',_{irms}$, for the Reynolds numbers examined, which are non-dimensionalized by inner variables, $\tau_w u_\tau/\nu$. For each Re_τ, the pressure derivatives show anisotropic behavior in the viscous and buffer regions, whereas those show isotropic behavior at $y^+ > 80$ where each component is almost the same magnitude. The Reynolds-number effect is noticeable in the viscous and buffer regions, while it is rather small in the outer layer, which is very similar to the Reynolds-number dependence on the vorticity fluctuations (Moser et al., 1999).

As shown in Figs. 1 and 2, the significant increases in p'_{rms} and $p',_{irms}$ occur near the wall. One may wonder if these increases show any specific functional dependence. To examine this issue, the limiting values of the mean-square values of p'^2_{rms}/τ_w^2 and $p',^2_{irms}/(\tau_w u_\tau/\nu)^2$ are given in Fig. 3. It is shown in Fig. 3 that the increasing rate for the limiting value of p'^2_{rms}/τ_w^2 is indeed significant for the Reynolds numbers investigated, whereas that for the limiting value of $p',^2_{irms}/(\tau_w u_\tau/\nu)^2$ seems to be rather saturated at $Re_\tau = 1020$. Interestingly, the increasing rate for the limiting value of p'^2_{rms}/τ_w^2 is almost proportional to the logarithmic function of the Reynolds number, i.e. $log(Re_\tau)$, which is consistent with the analyses of Bradshaw (1967) and Townsend (1976). Also, comparing the present results with those of Spalart (1988), the present results show much smaller values than those of Spalart (1988), which must be due to the difference in the outer layers between the channel and the boundary layer.

Figure 4 shows one-dimensional streamwise and spanwise wavenumber spectra of the wall pressure fluctuations for $Re_\tau = 180$, 395, 640 and 1020 nondimensionalized by inner variables, $\tau_w^2\nu/u_\tau$, where the spectra are defined as

$$\int_0^\infty \phi(k_x)dk_x = \int_0^\infty \phi(k_z)dk_z = p'^2_{rms}. \qquad (1)$$

Note that $\phi(k_x)$ and $\phi(k_z)$ the power spectra, and k_x and k_z are the wavenumbers in the x and z directions, respectively. In Fig. 4, the frequency spectrum measured by Nepomuceno and Lueptow (1997) at $Re_\tau = 751$ is also plotted for comparison, using Taylor's hypothesis with a convection velocity of $0.72U_0$ (Choi and Moin, 1990), where U_0 is the freestream velocity or channel centerline velocity. With this normalization, it is shown in both the streamwise and spanwise spectra that the power increases significantly with increasing Reynolds number at low wavenumbers, whereas the power does not increase appreciably with increasing Reynolds number at high wavenumbers, which agrees with the findings of Choi and Moin (1990) in the spectral scaling argument. The noticeable Reynolds-number effect at low wavenumbers corresponds to the significant increase in the rms value with increasing Reynolds number. Also, in Fig. 4, no apparent inertial sublayer appears for the Reynolds numbers examined. Nevertheless, p'^2_{rms}/τ_w^2 shows the logarithmic functional dependence with increasing Reynolds number (Fig. 3). Since the logarithmic relation is derived from the assumption of the k^{-1} range, there may exist another reason for the logarithmic increase in p'^2_{rms}/τ_w^2 with Re_τ.

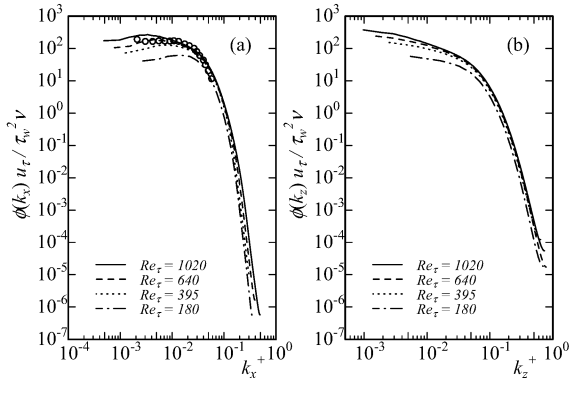

Figure 4: One-dimensional wavenumber power spectra of the wall pressure fluctuations for $Re_\tau = 180$, 395, 640 and 1020 normalized by wall units: (a) streamwise; (b) spanwise. ∘ , Nepomuceno and Lueptow ($Re_\tau = 751$).

In Fig. 4(a), clear peaks appear at low wavenumbers in the streamwise spectra for the Reynolds numbers examined, which may be closely associated with the global characteristics of the pressure. To see this behavior more clearly, the streamwise spectra shown in Fig. 4(a) are again plotted in linear scales at $k_x\delta < 50$, and are given in Fig. 5. Indeed, large peaks appear at low wavenumbers, $k_x\delta = 2.5 \sim 3.4$, for the given Reynolds numbers. The corresponding wavelengths are about $1.8 \sim 2.5\delta$, which may suggest that the origin of the peak exist in the outer layer.

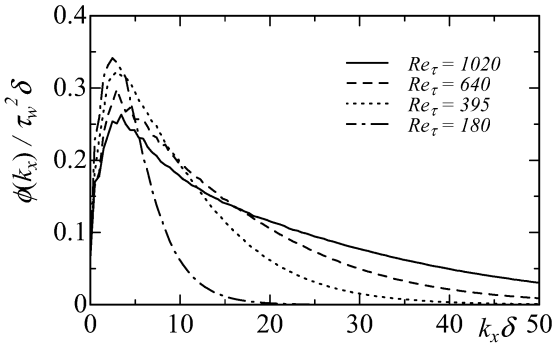

Figure 5: One-dimensional streamwise wavenumber power spectra of the wall pressure fluctuations for $Re_\tau = 180$, 395, 640 and 1020 normalized by $\tau_w^2\delta$ at $k_x\delta < 50$.

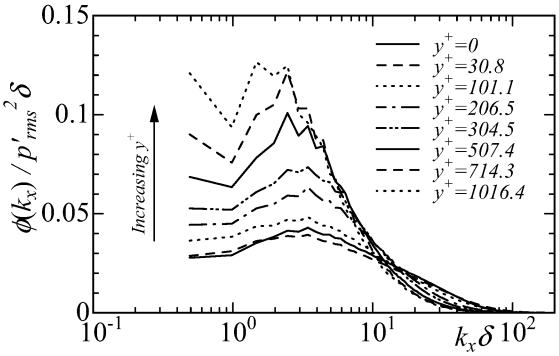

Figure 6: Streamwise wavenumber power spectra of the pressure fluctuations for $Re_\tau = 1020$ normalized by $p'^2_{rms}\delta$.

To examine the origin of the spectral peaks shown in Fig. 5, the streamwise wavenumber power spectra for $Re_\tau = 1020$ at several y locations are normalized by ${p'}^2_{rms}\delta$, and are given in Fig. 6, where the integration of the spectrum over the whole wavenumbers corresponds to unity. In Fig. 6, the spectrum at the wall shows almost the same behavior as that at $y^+ = 30$, indicating that the major contribution to the wall pressure comes from the buffer region (Kim, 1989; Johansson et al., 1991). With increasing distance from the wall, the power becomes more prominent at low wavenumbers, and noticeable peaks appear at $k_x\delta = 2.5 \sim 3.4$ throughout the channel, suggesting that there exists close association in the low-wavenumber behavior between the inner and outer layers.

In the following, we use the pressure splitting method such as the slow and rapid parts in order to investigate the global phenomena of the pressure at $Re_\tau = 1020$ in detail. Also, the total pressure is obtained directly from computing the Poisson equation to make thorough comparisons among the three types of the pressure, although the total pressure obtained from the Poisson equation does not show any noticeable difference to the total pressure as shown in Figs. 1$\sim$ 6.

The total, slow and rapid pressure at $Re_\tau = 1020$ is obtained by computing the Poisson equation using the data set of 50 consecutive instantaneous fields at a time interval of $\Delta t^+ \approx 3$. The Poisson equations of the total (p_t), slow (p_s) and rapid (p_r) pressure are expressed as

$$\nabla^2 p_t^+ = -\frac{\partial u_i^+}{\partial x_j^*} \cdot \frac{\partial u_j^+}{\partial x_i^*}, \tag{2}$$

$$\nabla^2 p_s^+ = -\frac{\partial u_i'^+}{\partial x_j^*} \cdot \frac{\partial u_j'^+}{\partial x_i^*}, \tag{3}$$

$$\nabla^2 p_r^+ = -2\frac{\partial v'^+}{\partial x^*} \cdot \frac{d\bar{u}^+}{dy^*}. \tag{4}$$

In Eqs. (2)$\sim$(4), the Neumann boundary condition is employed at the wall. For the rapid pressure, the homogenous boundary condition, $\partial p_r^+/\partial y^*|_w = 0$, is used, whereas for the total and slow pressure, the inhomogeneous boundary conditions, $\partial p_t^+/\partial y^*|_w = (1/Re_\tau) \cdot \left(\partial^2 v^+/\partial y^{*2}\right)|_w$ and $\partial p_s^+/\partial y^*|_w = (1/Re_\tau) \cdot \left(\partial^2 v'^+/\partial y^{*2}\right)|_w$, are used. The Stokes pressure (Mansour et al., 1988) is included in p_s.

Figure 7 shows the rms values of the total, slow and rapid pressure at $Re_\tau = 1020$. Near the wall, the rms values of the rapid and slow pressure are almost the same magnitude at $y^+ < 10$ where the linear and nonlinear interactions make nearly the same contribution to the wall pressure. Also, the contribution from the slow and rapid pressure to the total pressure is about 70 percent, which agrees with the result of Kim (1989) at $Re_\tau \approx 400$. In the center of the channel, on the other hand, the rms values of the total and slow pressure are almost the same magnitude, and the contributions from the rapid and slow pressure to the total pressure are about 40 and 95 percent, respectively.

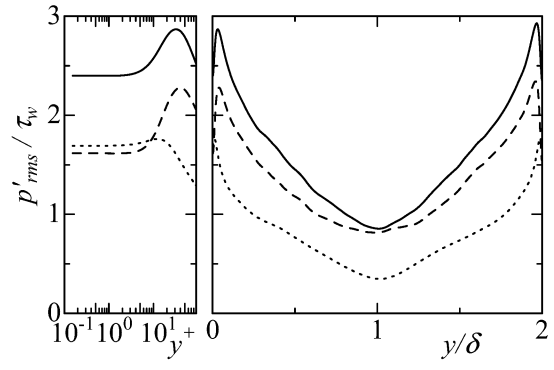

Figure 7: Root-mean-square value of the total, slow and rapid pressure fluctuations for $Re_\tau = 1020$ obtained from 50 instantaneous realizations with a time increment of $\Delta t^+ \approx 3$. ——, total; - - - - -, slow; · · · · ·, rapid.

The streamwise wavenumber power spectra of the total, rapid and slow pressure at $Re_\tau = 1020$ are given in Fig. 8. For the slow pressure, the spectra show almost the same behavior as those of the total pressure throughout the channel. Notably, the similarity is very high in the channel center where the flow reaches the isotropy state. For the rapid pressure, on the other hand, the power decreases noticeably at intermediate and high wavenumbers with increasing distance from the wall. In the center of the channel, a clear peak appears at a low wavenum-

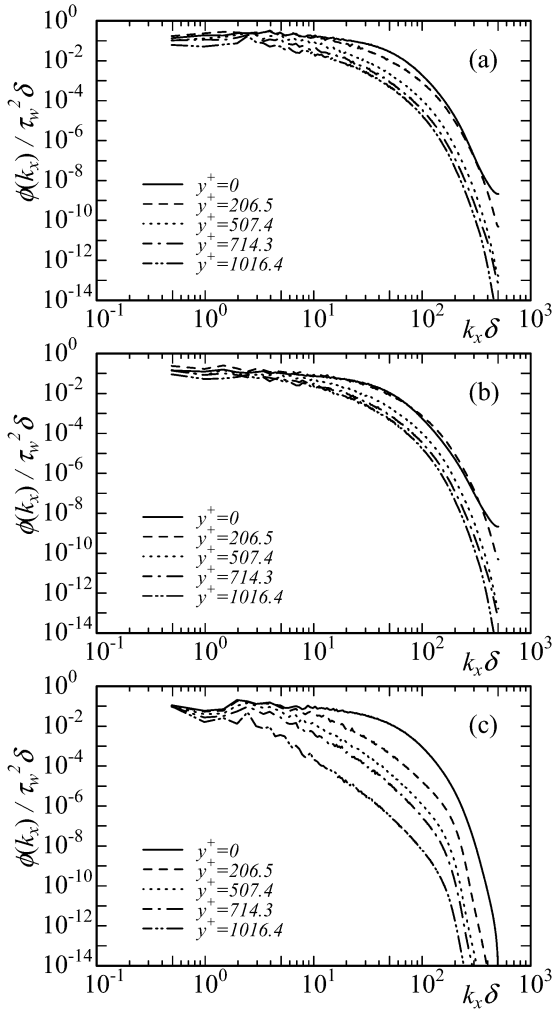

Figure 8: One-dimensional streamwise wavenumber power spectra of the rapid and slow pressure fluctuations for $Re_\tau = 1020$ normalized by τ_w and δ obtained from 50 instantaneous realizations with a time increment of $\Delta t^+ \approx 3$: (a) total; (b) slow; (c) rapid.

ber, $k_x\delta \approx 2.5$, which is persistent throughout the channel. The same trend also appears in the streamwise spectra of the total pressure, which agrees with the spectral behavior as shown in Fig. 6. This indeed suggests the close association in the low-wavenumber behavior between the total and rapid pressure. Hence, the origin of the peak in the streamwise spectra of the wall pressure fluctuations is attributed to the large peak in those of the rapid pressure in the outer layer.

Kim (1989) has already reported the persistent spectral peak of the rapid pressure at $Re_\tau = 180$, and indicated that the peak wavenumber is $k_x\delta = 1.5$. His wavenumber is smaller than that of the present study. We consider this difference to be due to the different sampling time periods between the two studies because longer time integration is required to obtain static turbulence statistics related to large scales (del Álamo and Jiménez, 2003; Abe et al, 2004b).

Contours of the instantaneous total, slow and rapid pressure fluctuations for $Re_\tau = 1020$ at the wall and in the channel center are shown in Figs. 9 and 10. At the wall (Fig. 9), we see a large number of positive and negative pressure fluctuations for the each pressure, where dominant length scales are almost the same size independently of the pressure type. Interestingly, large-scale patterns appear in the instantaneous total and rapid pressure at $Re_\tau = 1020$, which are elongated in the z direction with a streamwise spacing of about 2δ. The streamwise spacing agrees with the peak wavenumber as shown in Fig. 5. In the center of the channel (Fig. 10), on the other hand, the instantaneous rapid pressure shows the largest scales among the three types of the pressure, which are elongated in the z direction with a streamwise spacing of about 2δ. A comparison between Fig. 9(c) and Fig. 10(c) shows that the large-scale structures in the channel center occur at almost the same locations as the large-scale patterns at the wall, suggesting close relation between the two structures in the instantaneous rapid pressure.

To examine this issue further, contours of the instantaneous total, slow and rapid pressure fluctuations for $Re_\tau = 1020$ in the $x - y$ plane are given in Fig.11. Indeed, large-scale structures of the instantaneous rapid pressure appear in the outer layer, which are deep in the y direction and extend to the near-wall region. This again indicates the close association between the inner and outer-layer structures in the rapid pressure. Hence, the large-scale patterns in the instantaneous wall pressure fluctuations are essentially associated with the large-scale structures of the instantaneous rapid pressure in the outer layer, which causes the noticeable peaks in the streamwise spectra at low wavenumbers.

Interestingly, comparing the instantaneous slow and rapid

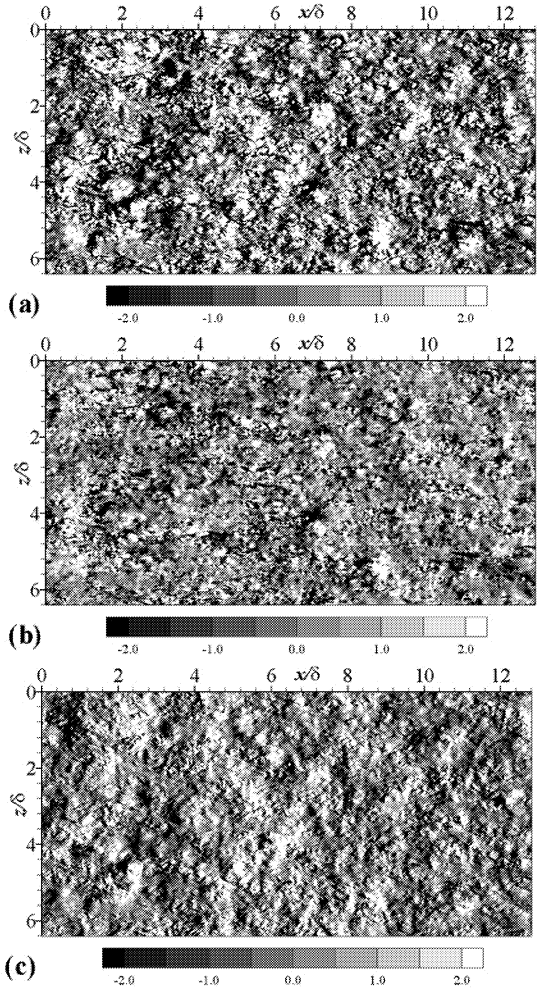

Figure 9: Contours of the instantaneous pressure fluctuations for $Re_\tau = 1020$ at the wall: (a) total; (b) slow; (c) rapid.

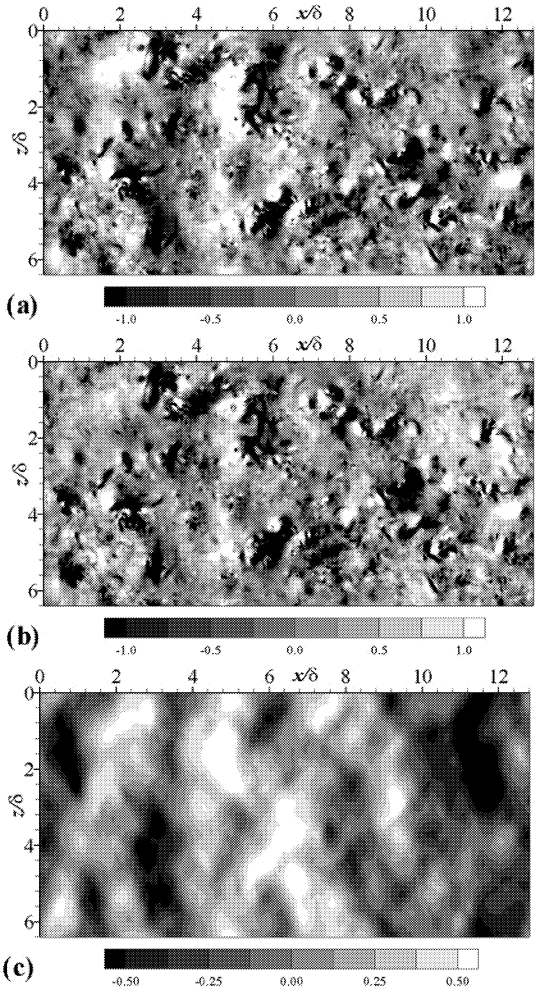

Figure 10: Contours of the instantaneous pressure fluctuations for $Re_\tau = 1020$ at $y/\delta = 1$: (a) total; (b) slow; (c) rapid.

pressure, the instantaneous slow pressure shows shear-layer structures near the wall, while the instantaneous rapid one shows large-scale structures that do not show any inclination to the wall (see Figs. 11(b) and 11(c)).

CONCLUSIONS

In the present study, DNS of a turbulent channel flow was performed at four Reynolds numbers, Re_τ = 180, 395, 640 and 1020 to investigate the Reynolds-number dependence on the pressure fluctuations. It was shown that the significant increases in the rms value of p' and $p'_{,irms}$ occur near the wall. Indeed, the increasing rate for the limiting value of p'_{rms} is significant, and p'^2_{rms}/τ_w^2 is almost proportional to $log(Re_\tau)$ for the Reynolds numbers examined.

It was shown in the streamwise spectra of the wall pressure fluctuations that large peaks appear at low wavenumbers, $k_x\delta = 2.5 \sim 3.4$, for the Reynolds numbers investigated. The origin of the peaks was examined using the pressure splitting method such as the rapid and slow parts at Re_τ = 1020. A closer examination revealed that large-scale patterns appear in the instantaneous wall pressure fluctuations at Re_τ = 1020, and they are essentially associated with large-scale structures of the instantaneous rapid pressure in the outer layer, which caused the noticeable peaks in the streamwise spectra of the wall pressure fluctuations at low wavenumbers.

AKNOWLEDGEMENT

The present work is based on the former work on the wall pressure fluctuations, in which the contribution by Prof. H. Choi of Seoul National University was significant. Computations were made with the use of Numerical Simulator III at Computer Center of Japan Aerospace Exploration Agency, and also VPP5000 at Tokyo University of Science and Computer Center of Kyushu University.

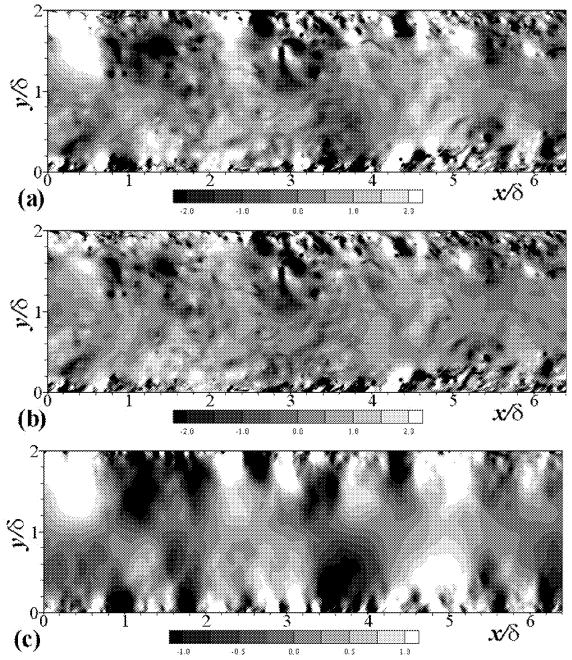

Figure 11: Contours of the instantaneous pressure fluctuations for Re_τ = 1020 in the $x-y$ plane: (a) total; (b) slow; (c) rapid.

REFERENCES

Abe, H., Kawamura, H. and Matsuo, Y., 2001, " Direct numerical simulation of a fully developed turbulent channel flow with respect to the Reynolds number dependence," *ASME J. Fluids Eng.*, Vol. 123, pp. 382-393.

Abe, H., Kawamura, H. and Matsuo, Y., 2004a, " Surface heat-flux fluctuations in a turbulent channel flow up to Re_τ = 1020 with Pr = 0.025 and 0.71," *Int. J. Heat and Fluid Flow*, Vol. 25, pp. 404-419.

Abe, H., Kawamura, H. and Choi, H., 2004b, " Very large-scale structures and their effects on the wall shear-stress fluctuations in a turbulent channel flow up to Re_τ = 640," *ASME J. Fluids Eng.*, Vol. 126, pp. 835-843.

Antonia, R. A. and Kim, J., 1994, " Low-Reynolds-number effects on near-wall turbulence," *J. Fluid Mech.*, Vol. 276, pp. 61-80.

del Álamo, J. C. and Jiménez, J., 2003, " Spectra of the very large anisotropic scales in turbulent channels," *Phys. Fluids*, Vol. 15, L41-L44.

del Álamo, J. C., Jiménez, J., Zandonade, P., and Moser, R. D., 2004, " Scaling of the energy spectra of turbulent channels," *J. Fluid. Mech.*, Vol. 500, pp. 135-144.

Bradshaw, P., 1967, " Inactive' motion and pressure fluctuations in turbulent boundary layers," *J. Fluid Mech.*, Vol. 30, 241-258.

Choi, H. and Moin, P., 1990, " On the space-time characteristics of wall pressure fluctuations," *Phys. Fluids*, Vol. A 2, pp. 1450-1460.

Eckelmann, H., 1989, " A review of knowledge on pressure fluctuations," In: *Near-Wall Turbulence*, Kline, S. J. and Afgan, N. H., eds., Hemisphere, New York, pp. 328-347.

Hu, Z., Morfey, C. L., and Sandham, N. D., 2003, " Sound radiation in turbulent channel flows," *J. Fluid. Mech.*, Vol. 475, pp. 269-302.

Johansson, A. V., Alfredsson, P. H. and Kim, J., 1991, " Evolution and dynamics of shear-layer structures in near-wall turbulence," *J. Fluid. Mech.*, Vol. 224, pp. 579-599.

Kawamura, H., Abe, H. and Matsuo, Y., 1999, " DNS of turbulent heat transfer in channel flow with respect to Reynolds-number effect," *Int. J. Heat and Fluid Flow*, Vol. 20, pp. 196-207.

Kim, J., 1989, " On the structure of pressure fluctuations in simulated turbulent channel flow," *J. Fluid. Mech.*, Vol. 205, pp. 421-451.

Mansour, N. N., Kim. J. and Moin, P., 1988, " Reynolds-stress and dissipation-rate budgets in a turbulent channel flow," *J. Fluid. Mech.*, Vol. 194, pp. 15-44.

Moser, R. D., Kim, J. and Mansour, N. N., 1999, " Direct numerical simulation of turbulent channel flow up to Re_τ = 590," *Phys. Fluids*, Vol. 11, pp. 943-945.

Nepomuceno, H. G. and Lueptow, R. M., 1997, " Pressure and shear stress measurements at the wall in a turbulent boundary layer on a cylinder," *Phys. Fluids*, Vol. 9, pp. 2732-2739.

Spalart, P. R., 1988, " Direct simulation of a turbulent boundary layer up to R_θ = 1410," *J. Fluid. Mech.*, Vol. 187, pp. 61-98.

Townsend, A. A., 1976, " The structure of turbulent shear flows," 2nd edition, Cambridge University Press.

Willmarth, W. W., 1975, " Pressure fluctuations beneath turbulent boundary layers," *Ann. Rev. Fluid. Mech.*, Vol. 7, pp. 13-88.